Predictability of an Advection Fog Event over North China. Part I: Sensitivity to Initial Condition Differences

HUIQIN HU, QINGHONG ZHANG, BAOGUO XIE, YUE YING,* AND JIPING ZHANG[+]

*Laboratory for Climate and Ocean–Atmosphere Studies, Department of Atmospheric and Oceanic Sciences,
School of Physics, Peking University, Beijing, China*

XIN WANG

National Satellite Meteorological Center, China Meteorological Administration, Beijing, China

ABSTRACT

The predictability of a dense advection fog event on 21 February 2007 over north China (NC) is investigated with ensemble simulations using the Weather Research and Forecasting Model (WRF). Members with the best and worst simulation are selected from the ensemble, and their initial condition (IC) differences are explored. To test the sensitivity of fog simulation to those differences, the model is initialized with ICs that change linearly from the worst member to the best member, and the changes in simulated results are examined. The improvement in simulations due to the linear improvement of ICs is found to be monotonic. The IC differences at lower levels are of more influence to the simulation than IC differences at higher levels. By removing the IC differences of each meteorological variable individually, it is found that improvements in potential temperature and horizontal wind are more important than that of water vapor mixing ratio in this case. Additionally, the linear improvement in each meteorological variable also contributes monotonically to the simulated results. The budget analyses of the tendency of potential temperature and water vapor mixing ratio show that turbulence mixing and advection are the major factors contributing to the formation of fog. The correct initial temperature field ensures the formation and maintenance of an inversion, and the correct initial wind field ensures the correct transport of temperature and moisture in this case. Further discussion examines the reasons for the monotonic behavior in the simulation improvement.

1. Introduction

Fog is a weather phenomenon in which water or ice droplets suspended near the surface reduce the atmospheric horizontal visibility (AHV) to below 1 km (Glickman 2000). Fog can be highly problematic in some regions, and can result in losses to the local economy through its adverse impacts on human activity (Niu et al. 2010). The total economic loss in aviation, marine, and land transportation associated with fog can be comparable to that of tornadoes or even winter storms and hurricanes (Gultepe et al. 2007). Over north China (NC), fog is frequently observed in autumn and winter (Guo and Zhang 2007). Due to the increasingly heavy traffic in the NC region, fog has become a new type of high-impact weather event. The current ability to forecast fog is very limited due to the complexity, diversity, and finescale nature of the processes involved (Bergot and Guedalia 1994; Bergot et al. 2005; Zhou and Du 2010). A variety of models have been used to simulate fog-related events: from one-dimensional (1D) fog models such as the Code de Brouillard à l'échelle locale 1D boundary/fog model (Tardif 2007) and the microphysical fog model (von Glasow and Bott 1999) for local fog, to two-dimensional (2D) and three-dimensional (3D) models (Ballard et al. 1991), as well as coupled models [1D model of nocturnal boundary layer coupled with the land surface model; Muller (2006)] for regional fog. Large-eddy

---

* Current affiliation: *Department of Meteorology, The Pennsylvania State University, University Park, Pennsylvania.*

+ Current affiliation: *Beijing Institute of Applied Meteorology, and Institute of Atmospheric Physics, Chinese Academy of Sciences, Beijing, China.*

Corresponding author address: Dr. Qinghong Zhang, Dept. of Atmospheric and Oceanic Sciences, School of Physics, Peking University, Beijing 100871, China.
E-mail: qzhang@pku.edu.cn

simulation (LES) has also been utilized to study the 3D structure of fog (Nakanishi 2000). In particular, the Weather Research and Forecasting Model (WRF) has been successfully implemented to simulate fog (Muller 2006; Van der Velde et al. 2010; Zhou and Du 2010) and has shown potential for sea fog simulation (Gao et al. 2010) and the forecasting of advection fog (Li et al. 2007). However, the current performance of operational fog forecasts at the National Centers for Environmental Prediction (NCEP) is much lower than that of predictions for precipitation from the same models (Zhou 2011). Such low performance is due to a lack of understanding of the predictability of fog, since most studies of weather predictability currently focus only on synoptic or convective weather, or cyclones (Melhauser and Zhang 2012; Van Sang et al. 2008; Walser et al. 2004; Zhang et al. 2003; Zhang et al. 2006).

In recent years, the predictability of fog has begun to draw the attention of some researchers. Studies have investigated the influences on fog simulation of turbulence (Nakanishi 2000; Welch et al. 1986), terrain (Golding 1993), vegetation (Duynkerke 1991; von Glasow and Bott 1999), and model resolution (Ballard et al. 1991; Chibe and Cotton 2003; Muller 2006; Tardif 2007; Van der Velde et al. 2010). To improve the predictability and obtain better forecasts, ensemble methods are introduced, such as the multimodel ensemble forecast (Muller 2006; Muller et al. 2007), the Local Ensemble Prediction System (LEPS; Roquelaure and Bergot 2008), the multimodel-based Mesoscale Ensemble Prediction System (MEPS; Ryerson 2012), and the National Centers for Environmental Prediction's (NCEP) Short-Range Ensemble Forecast System (SREF; Zhou and Du 2010; Zhou et al. 2012). Ensemble forecasts have proved to be effective in providing a meaningful measure of forecast uncertainty. Studies for evaluating the sensitivity of fog simulation to changes (errors) in the initial conditions (ICs) have also been conducted by, among others, Fitzjarrald and Lala (1989) and Musson-Genon (1987). The methods that determine the sensitivity to ICs can be based on either an adjoint model (Errico and Vukicevic 1992) or an ensemble of model runs (Ancell and Hakim 2007; Melhauser and Zhang 2012; Torn and Hakim 2008, 2009; Wu et al. 2013). For fog events, Bergot and Guedalia (1994) used a 1D model to study the sensitivity of radiation fog to ICs. The sensitivity of a dense fog event to the ICs is investigated with the fifth-generation Pennsylvania State University–National Center for Atmospheric Research Mesoscale Model (MM5; Pagowski et al. 2004). Ballard et al. (1991) conducted a series of tests to investigate the sensitivity of sea fog to the ICs using the Met Office (UKMO) mesoscale model.

Fog is a threshold phenomenon in the planetary boundary layer (PBL). During its maintenance, cooling, turbulence, advection, droplet sedimentation, etc. all play critical roles but remain in balance. Zhou and Ferrier (2008) identified an explicit balance threshold among these processes and its relationship to the profiles of temperature and relative humidity (RH). This relationship was extended to include wind and moisture advection (Zhou 2011). Therefore, an appropriate PBL scheme and a set of error-free initial temperature, RH, and wind conditions are crucial for the successful simulation or forecasting of a fog event. Unfortunately, the PBL schemes that can be selected in the current WRF suite are not specifically designed for fog, and ICs are far from error free. Roman-Cascon et al. (2012) conducted several sensitivity tests for three PBL schemes [Mellor–Yamada–Janjić (MYJ), quasi-normal scale elimination (QNSE), and Mellor–Yamada–Nakanishi–Niino (MYNN)] used in version 3.3 of the Advanced Research core of WRF for selected winter fog events and found that the performance of these three schemes was case dependent, although MYNN performed slightly better than the others. Therefore, temperature, RH, and wind are the meteorological variables selected to explore the sensitivity of fog simulations to IC differences in this study.

In addition to the previous studies, this paper attempts to test the predictability of a dense advection fog event. We use an approach similar to that of Melhauser and Zhang (2012). To the authors' knowledge, this is the first attempt to study the sensitivity of fog simulation to differences in the ICs using an ensemble-based method. The advection fog case selected for this study is different from either the sea fog or radiation fog in the aforementioned studies. Insights from the sensitivity analyses will be beneficial to our understanding of the phenomenon and the potential improvement to the observation network. The Chinese government is planning to build a new surface observation network over the NC area to improve its fog forecasting capacity; so this study is also the first attempt to determine what types of instruments will be required and where the observation stations are needed over NC. This paper is organized as follows. A case overview is presented in section 2, followed by the experimental design in section 3. Section 4 describes the validation methods. Section 5 consists of two parts: the first part will present fog simulation results and the second part will explore the sensitivity of the fog simulation to IC differences in detail. Section 6 presents the discussion. The summary is given in section 7.

2. Case overview

At 1930 UTC 20 February 2007 [0330 local standard time (LST) 21 February 2007], fog was observed in the
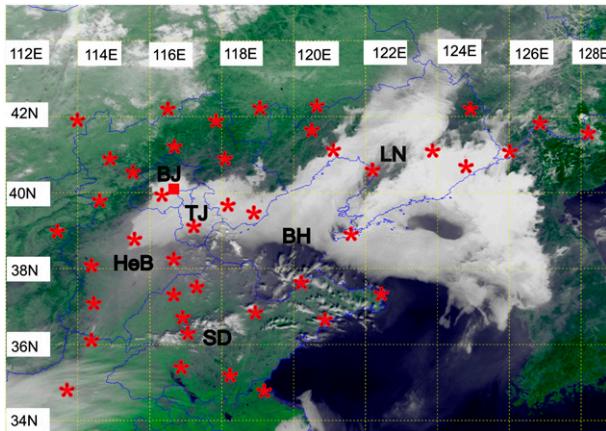
FIG. 1. Satellite visible image from *NOAA-17* at 0228 UTC 21 Feb 2007 (http://rsapp.nsmc.cma.gov.cn/is_nsmc/info_service/fog/fogView.aspx?id=B20070221000012000400010241024), and locations of the 42 meteorological surface stations (red asterisks; the location of BCA is marked as a square red symbol). The gray-filled region with a sharp boundary indicates the fog coverage area.

NC area, which includes eastern Hebei Province (HB) and Beijing (BJ), most of Tianjin (TJ) and Liaoning Province (LN), the Bohai Sea (BH), and the northern Yellow Sea (YS) (Liang et al. 2009). Visible imagery from the *National Oceanic and Atmospheric Administration-17* (*NOAA-17*) polar-orbiting meteorological satellite (http://rsapp.nsmc.cma.gov.cn/is_nsmc/info_service/fog/fogView.aspx?id=B20070221000012000400010241024; Fig. 1) indicated that NC and most of the BH were covered by fog at 0228 UTC 21 February 2007. The AHV at Beijing Capital Airport (BCA, location shown in Fig. 1) was reduced to less than 50 m during the period from 1930 UTC 20 February to 0600 UTC 21 February 2007 (Liang et al. 2009). Due to the intrusion of cold air from the northeast at 2000 UTC 21 February 2007, the fog began to dissipate, and the AHV observed at BCA gradually increased to above 2 km (Liang et al. 2009).

This fog event lasted more than 24 h and caused the cancellation of 234 flights, and further delayed more than another 500 flights with over 30 000 travelers stranded at the BCA (Liang et al. 2009). A newspaper reported that "dense fog raided Beijing" (http://news.sina.com.cn/c/2007-02-22/003311272907s.shtml) due to the unsuccessful forecast of this fog event.

NCEP Final Analysis (FNL) data with horizontal resolution of $1° \times 1°$ are used for synoptic analysis based on the heights at 500 hPa (Figs. 2a,b) and sea level pressure, surface wind, and RH (Figs. 2c,d). At 500 hPa, as shown in Fig. 2a, there was a ridge of high pressure downstream of Baikal Lake (the location shown in Fig. 2a) at 1200 UTC 20 February 2007. The ridge moved slowly eastward, and dominated NC at 0000 UTC

21 February 2007. At the same time, a weak cold trough of low pressure moved over Baikal Lake from the west (Fig. 2b). The stable upper-level circulation was suitable for fog formation and propagation. At the surface, NC was dominated by the transition zone of a weak high to the east and a low to the west with a weak horizontal pressure gradient (Figs. 2c,d). The moisture over YS and BH was transported to NC in an anticyclonic path along the south edge of the high at the surface. Moreover, the southerly and easterly winds over NC supplied abundant moisture and weak wind conditions, which were suitable for fog formation and maintenance (Liang et al. 2009).

3. Experimental design

WRF version 3.3.1 (Skamarock et al. 2008) is used in this study. Three nesting domains with horizontal resolutions of 27, 9, and 3 km, are implemented, as indicated in Fig. 3. The coarsest domain (D01) with 159 (west–east) and 153 (south–north) grid points provides coverage of the synoptic-scale environment. The finer domains (D02 and D03), with 232 and 448 (west–east) and 214 and 343 (south–north) grid points, respectively, cover the region where the fog event took place. The model top is at 50 hPa and there are 40 vertical levels with 7 levels below 1 km in the model.[1] Because vegetation has an important influence on fog formation (Duynkerke 1991), we use the 500-m land-use data as of the year 2000 (Zhang et al. 2007) for D03, which are more realistic than the conventional 30-arc-s U.S. Geological Survey (USGS) land-use data (Hitt 1994). As for parameterization schemes, the WRF single-moment 6-class microphysics scheme (Hong and Lim 2006), the Rapid Radiative Transfer Model (RRTM) longwave radiation scheme (Mlawer et al. 1997), the Dudhia shortwave radiation scheme (Dudhia 1989), and the QNSE PBL and surface layer schemes (Sukoriansky et al. 2005) are utilized in the simulation. The Kain–Fritsch cumulus scheme (Kain 2004) is used only for D01 and D02.

The deterministic simulation (DETS) is initialized at 0000 UTC 20 February 2007 and integrated until 0000 UTC 22 February 2007 with the initial and boundary conditions provided by NCEP 6-hourly FNL data. For the ensemble simulation (ENSS), similar to the method used by Wu et al. (2013), we generate ICs by randomly perturbing the initial field of DETS (the FNL data at 0000 UTC 20 February 2007). The perturbations are generated by randomly sampling the background

---

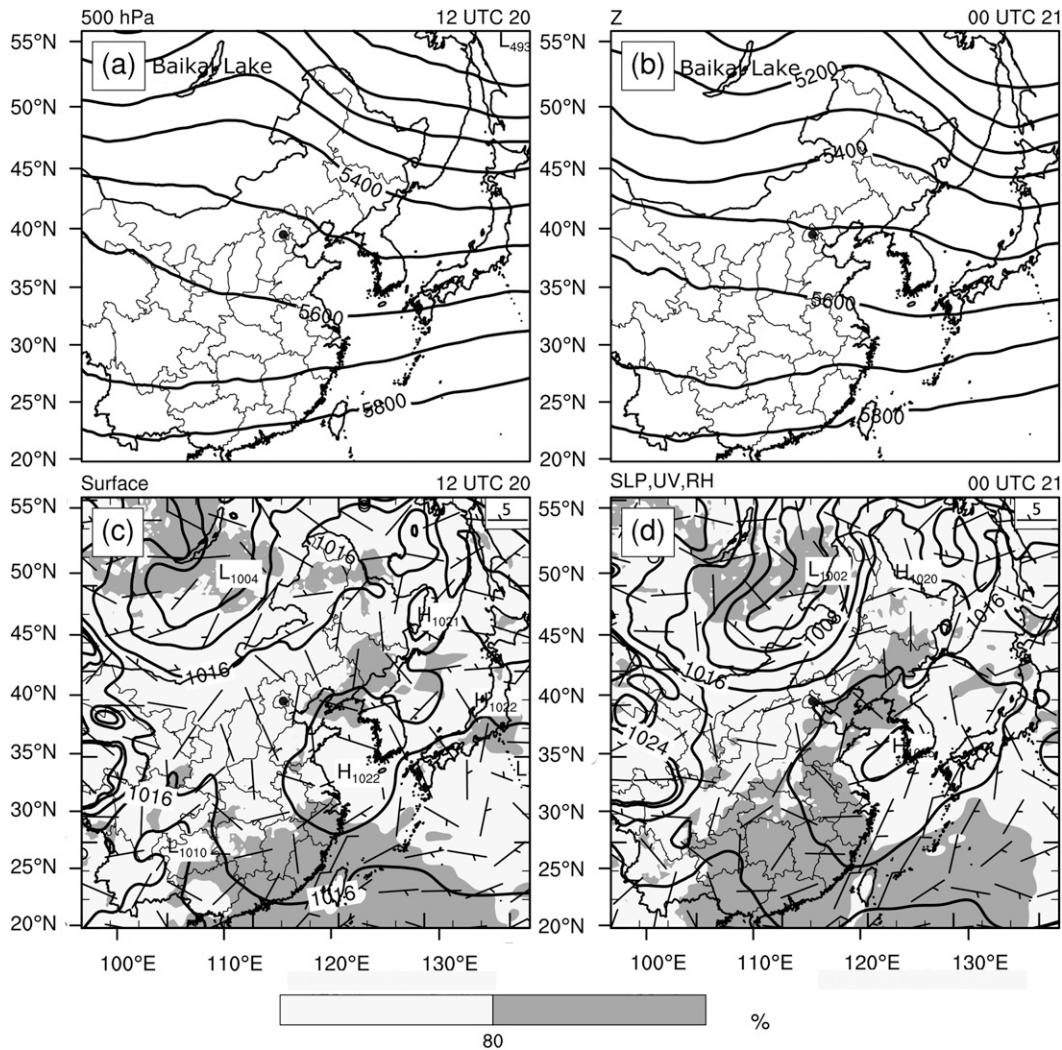[1] The heights are approximately 27, 94, 184, 299, 444, 630, and 859 m.

FIG. 2. Synoptic review of the fog event: 500-hPa heights at (a) 1200 UTC 20 Feb and (b) 0000 UTC 21 Feb 2007. Sea level pressure (contours every 4 hPa), 10-m wind (full barb = 5 m s^{-1}), and relative humidity (shading) at (c) 1200 UTC 20 Feb and (d) 0000 UTC 21 Feb 2007. Beijing is marked with a dot.

error covariance from the WRF-VAR fixed-covariance model (Skamarock et al. 2008). The standard deviations of the initial ensemble are roughly 0.3 g kg^{-1} for the water vapor mixing ratio, 3 m s^{-1} for wind, and 1.2 K for air temperature. The ENSS is an ensemble of 40 members with the boundary conditions, the basic model configurations, and parameterizations the same as in DETS.

In this paper, IC differences are defined as the differences in initial fields between members with the best (BSTM) and worst (WSEM) fog simulations (BSTM − WSEM). The BSTM and the WSEM are selected from the 40 ensemble members using the validation methods documented in section 4. To study the IC differences, the simulation is based on the assumption of a "perfect model" (Roquelaure and Bergot 2008). So except for the ICs, all of the sensitivity experiments are initialized at

0000 UTC 20 February 2007 and integrated for 48 h with the boundary conditions, the basic model configurations, and parameterizations the same as in DETS.

To evaluate the impact of IC differences on the simulation results, split experiments (SPTEXPs) are performed by dividing the IC differences into 10 equal parts, and then adding several to the ICs of the WSEM to create nine "intermediate" new ICs. We first apply these changes to all variables in the IC differences, and initialize nine runs (All_1, All_2, . . . , All_9), where All_n contains n/10 of the IC differences. This method is similar to that proposed by Melhauser and Zhang (2012). To study the vertical distributions of such sensitivity, replacement experiments (REPEXPs) are performed by adding the IC differences at the bottom 10 (~1.7 km, in height measured from the surface), 15 (~4.2 km),
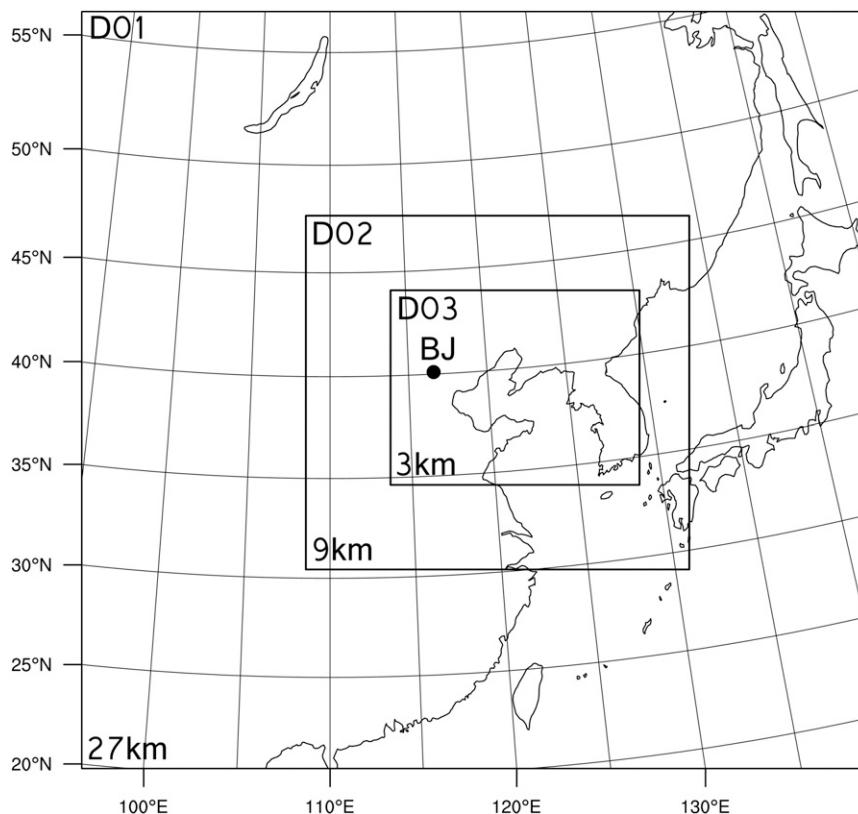
FIG. 3. Configuration of the nested model domains.

20 (~7 km), 25 (~9.8 km), and 30 (~13 km) vertical model levels to the IC of the WSEM and obtaining five corresponding simulations (L10, L15, L20, L25, and L30, respectively). To further explore the impact from each individual meteorological variable, removal experiments (RMVEXPs) are conducted by eliminating separately the IC differences of the water vapor mixing ratio (Qv), potential temperature (θ), and horizontal wind (U, V) at all vertical model levels from the IC of the BSTM and running seven new simulations based on these new ICs (RMV_Qv, RMV_θ, RMV_UV, RMV_Qvθ, RMV_QvUV, RMV_θ UV, and RMV_ Qvθ UV).

4. Validation methods

The performance of the simulations is evaluated through comparing the simulated fog coverage over NC against the coverage in the same regions retrieved from satellite detections (Fig. 1). Besides this subjective evaluation, the simulations are also validated quantitatively by some objective measures, such as the equitable threat score (ETS) and bias. To validate the simulation results quantitatively, AHV observations from both surface stations and *NOAA-17* are used. The 42 routine meteorological surface stations (locations shown in Fig. 1) provide 3-hourly data (station data) in D03 from 1200 UTC 20 February to 0000 UTC 22 February 2007. The satellite retrieval AHV data (satellite data) at 0228 UTC 21 February 2007 (http://rsapp.nsmc.cma.gov.cn/is_nsmc/ info_service/fog/fogindex.aspx?IsTopTen=False&Year= 2007&Month=2&Day=21.) have higher spatial resolution (1.27 km) and are interpolated to the nearest model grid point of D03 when used to compare with the model simulation at 0300 UTC 21 February 2007 (the mature stage of the fog event).

A low AHV value is an effective criterion for indicating whether fog is developing. As AHV is not a direct output from WRF, several codes are developed to calculate AHV based on the WRF output. The calculation of AHV in this study follows Kunkel (1984) and is based on the visibility–mixed-phase water content (MWC) relationship. The algorithm of AHV is as follows:

$$\text{AHV} = -1000 \times \ln(0.02)/\beta, \tag{1}$$

where the unit of AHV is meters and β is the extinction coefficient, which is calculated from the MWC by

$$\beta = 144.7 \text{MWC}^{0.88}, \tag{2}$$

where MWC $(g\,m^{-3})$ is the sum of water vapor, cloud ice, cloud water, snow, and rain.

Considering fog observations–simulation as binary events (1 = true, 0 = false), two measures (ETS and bias) can be used to validate the simulation:

$$ETS = \frac{H - R}{F + O - H - R} \qquad (3)$$

and

$$bias = \frac{F}{O}, \qquad (4)$$

where F = points with fog simulation, H = points with correct fog simulation (hits), O = points with fog observation ("reference" thereafter), and $R = F \times O/N$ is a random hit penalty, with N being the total number of grid points in the verification domain (Muller 2006; Muller et al. 2007; Zhou and Du 2010; Zhou et al. 2012). As bias is defined as the ratio of total fog-simulated points to total fog-observed points, the ideal value for the bias is 1 (the numbers of observation and simulation points are about the same), and over- (under-) prediction is indicated by bias greater (less) than 1. The larger ETS is, the better performance the simulation has.

To validate DETS and ENSS, ETS and bias are calculated for model AHV output against station data from the temporal aspect and satellite data from the spatial aspect. From the temporal aspect, we use the 3-hourly simulated AHV at the lowest model level (lev1, ~27 m) for the 42 meteorological stations in D03 from 1200 UTC 20 February to 0000 UTC 22 February 2007 to obtain the station ETS and station bias. It should be noted that, during the calculation of station ETS, N is the total number of points considering all 42 stations during the verification periods instead of in the verification domain. From the spatial aspect, we use the simulated AHV at the third vertical model level (lev3, ~184 m) in D03 at 0300 UTC 21 February 2007 (closest model time to satellite data) to obtain satellite ETS and satellite bias. Because fog depth at the mature stage in this case was over 200 m (Liang et al. 2009) and the bird's-eye image of satellite detection is better than the traditional AHV at lev1 (Gao et al. 2010), we choose the simulated AHV at lev3 instead of at lev1 to obtain the ETS and bias based on the satellite retrieval AHV data.

To understand what aspects of IC differences are more important in fog simulation in this case, for the validation of the sensitivity experiments, BSTM is used as the reference when we calculate the ETS and bias from both the spatial and temporal aspects. In other words, for the calculation of ETS and bias from the spatial aspect, the satellite data are replaced by the simulated AHV at lev3
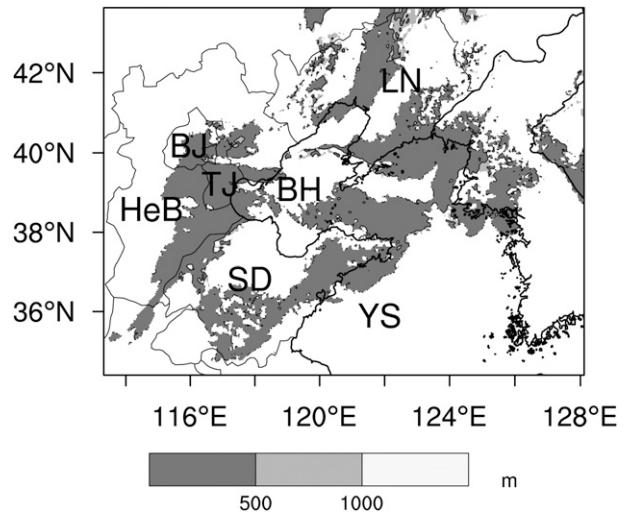

FIG. 4. The simulated fog coverage (area of AHV < 1 km in gray shading) obtained from D03 at 0300 UTC 21 Feb 2007 at lev3 for the DETS.

in D03 at 0300 UTC 21 February 2007 from the BSTM, and for the calculation of ETS and bias from the temporal aspect, the station data are replaced by the 3-hourly simulated AHV at lev1 for the 42 meteorological stations in D03 from 1200 UTC 20 February to 0000 UTC 22 February 2007 from the BSTM. In the following analysis of sensitivity experiments, we can obtain similar results from the ETS and bias (sim-ETS and sim-bias) calculation at a particular time. Accordingly, we pay more attention to the spatial aspect in this paper. As a comparison, the ETS and bias of WSEM are also calculated from the spatial aspect by taking the BSTM as the reference (SWSEM-ETS and SWSEM-bias).

5. Results

a. Fog simulation results

The simulated fog coverage at 0300 UTC 21 February 2007 for DETS is shown in Fig. 4. There was false fog coverage over southern Shandong Province (SD) and southern BH. The fog coverage over the northern BH is less than the observation (Fig. 1). Quantitatively, the satellite ETS = 0.202 and satellite bias = 1.337 from the spatial aspect; station ETS = 0.087 and station bias = 2.408 from the temporal aspect. The simulation overpredicts this fog event. This indicates that DETS is unable to capture this fog event well and ENSS potentially could be very helpful for this case.

As for ensemble runs, ETS and bias are calculated for all 40 members. From the spatial aspect, members 5, 8, 14, 19, and 30 (M05, M08, M14, M19, and M30) score

FIG. 5. As in Fig. 4, but for the ENSS.

relatively higher (satellite ETS = 0.250, 0.250, 0.302, 0.202, and 0.257, respectively; satellite bias = 1.18, 1.07, 1.16, 1.05, and 1.22, respectively). From the temporal aspect, M08, M30, and M36 score relatively higher (station ETS = 0.109, 0.144, and 0.130, respectively;

station bias = 2.44, 2.24, and 2.08, respectively). Based on a combination of satellite ETS (satellite bias) and station ETS (station bias), M08 and M30 produced better scores than the other members, which is also illustrated by the simulated fog coverage at 0300 UTC 21
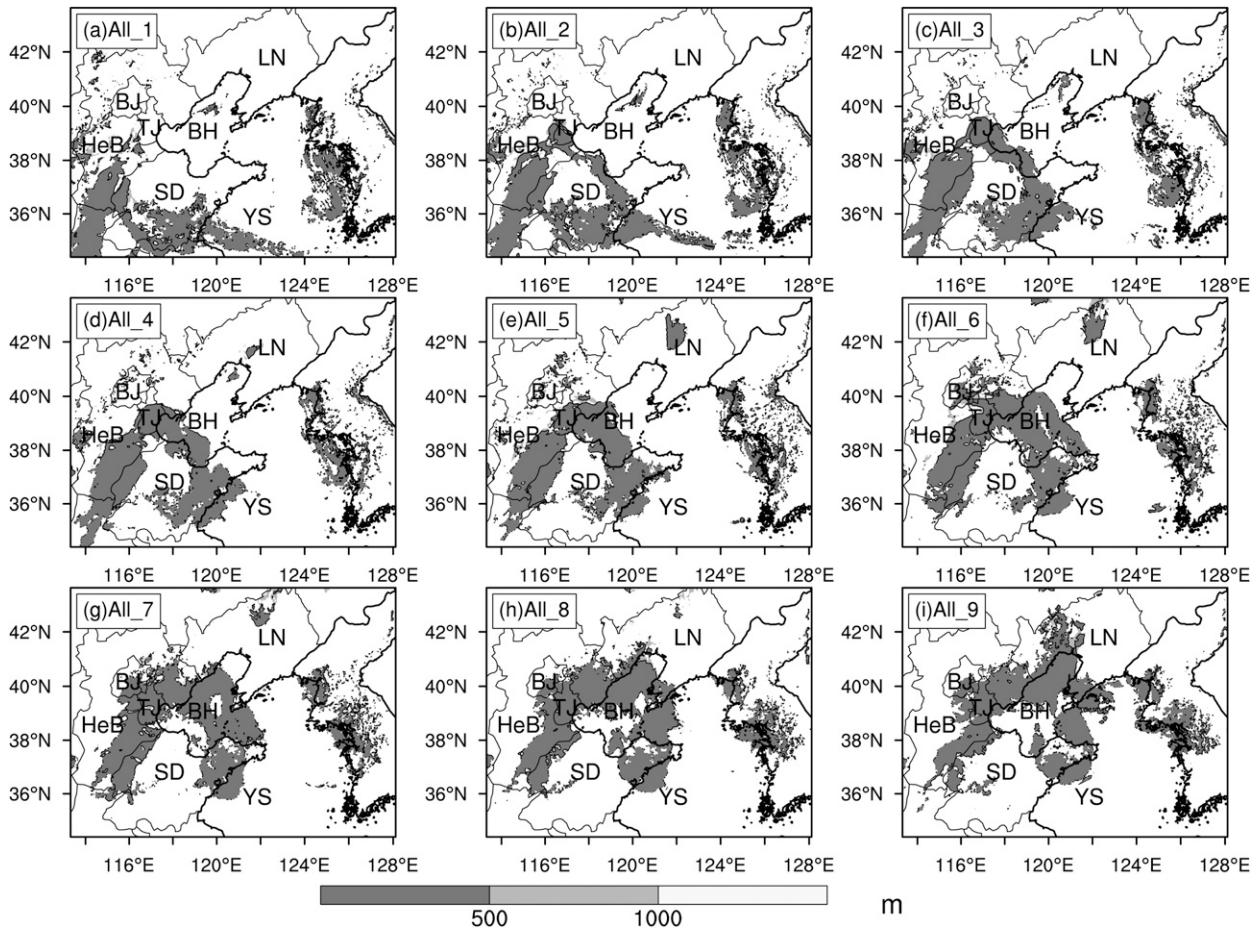
FIG. 6. As in Fig. 4, but for the experiments All_1 to All_9 in SPTEXP.

February 2007 (Fig. 5) where the simulation of these two members captured the observed fog coverage (Fig. 1). Although the satellite ETS and satellite bias of M08 and M30 are acceptable, the station ETS of these two members is still low, and the station bias is much greater than 1. This implies that fog predictability for this case is quite low. Similarly, M35 and M38 score lowest from both the spatial aspect (satellite ETS = −0.061 and −0.022, respectively; satellite bias = 0.83 and 0.72, respectively) and temporal aspect (station ETS = −0.016 and 0.068, respectively; station bias = 1.16 and 1.63, respectively). This is also illustrated by the simulated fog coverage at 0300 UTC 21 February 2007 (Fig. 5) where the simulation of those two members gave either false fog coverage or less fog coverage than the observation (Fig. 1). From Fig. 5, we verify that the simulated fog coverage of M08 does follow the observation (Fig. 1) very well. In contrast, the simulated fog coverage of M35 does not capture the event at all. Therefore, M08 and M35 are chosen as the BSTM and WSEM, respectively.

b. Sensitivity to IC differences

1) SPLIT EXPERIMENT (SPTEXP)

As fog occurs when the temperature and dewpoint temperature become identical (or almost identical) (Glickman 2000), it is possible that slight variations in the ICs would generate significant differences in the simulations. To explore the sensitivity of simulations to the linear improvement of ICs, the SPTEXP is conducted (documented in section 3).

Figure 6 shows the simulated fog coverage in All_1 to All_9. The improvement of the simulated fog coverage appears to be monotonic as IC varies linearly from the WSEM to the BSTM. The simulated fog coverage at 0300 UTC 21 February 2007 of experiments All_1 to All_9 changed from none over NC and BH to a pattern similar to that of the BSTM (Fig. 5). The false fog coverage that appeared over southern SD, northern Henan Province (HN), and YS in the WSEM also gradually improved toward the BSTM. Quantitatively, the sim-ETS (sim-bias) results for the WSEM and experiments
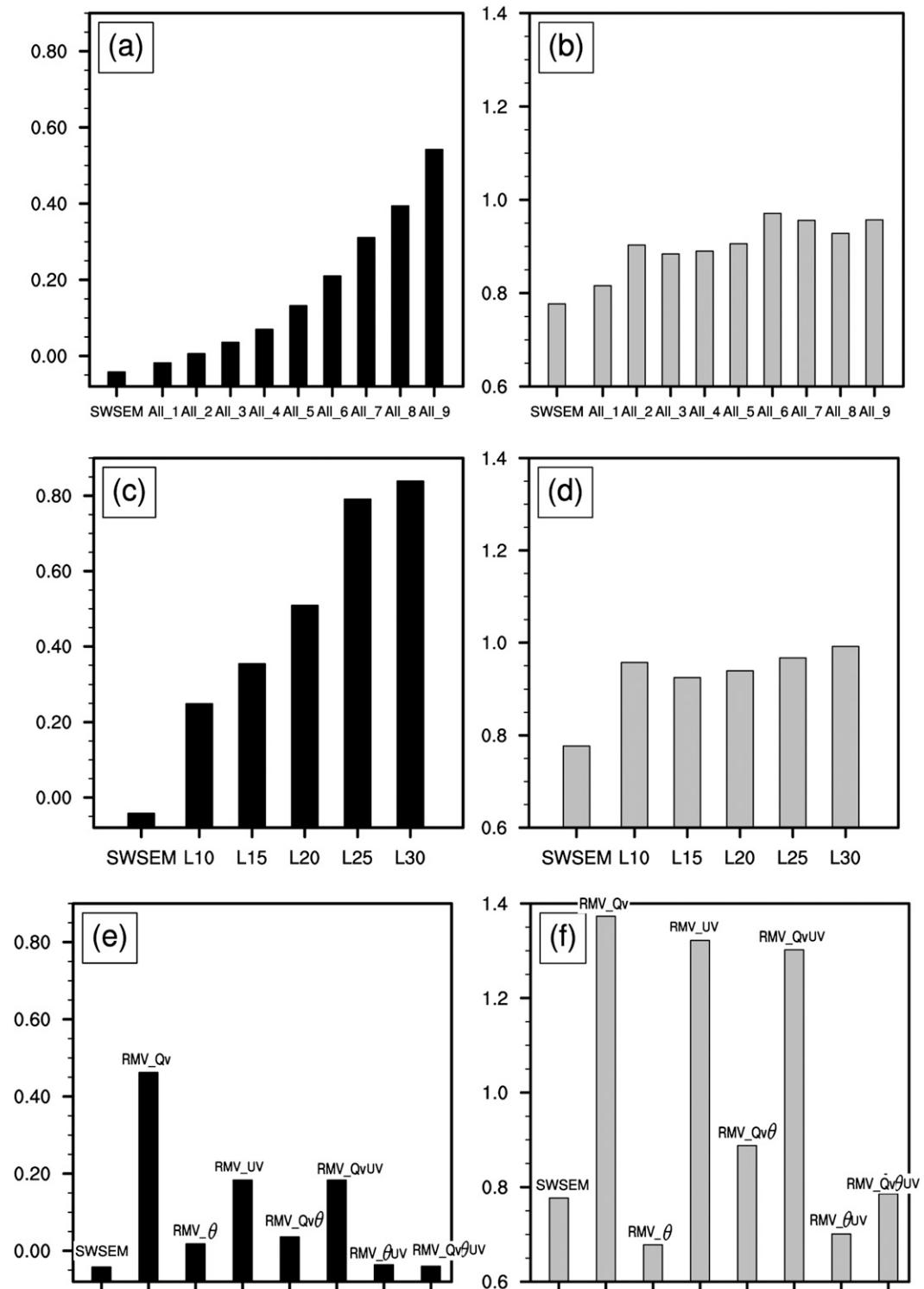
FIG. 7. The (left) sim-ETS and (right) sim-bias results calculated at 0300 UTC 21 Feb 2007 at lev3 for (a),(b) SPTEXP; (c),(d) REPEXP; and (e),(f) RMVEXP. The sim-ETS and sim-bias results for the WSEM (SWSEM) have also been plotted in each panel.
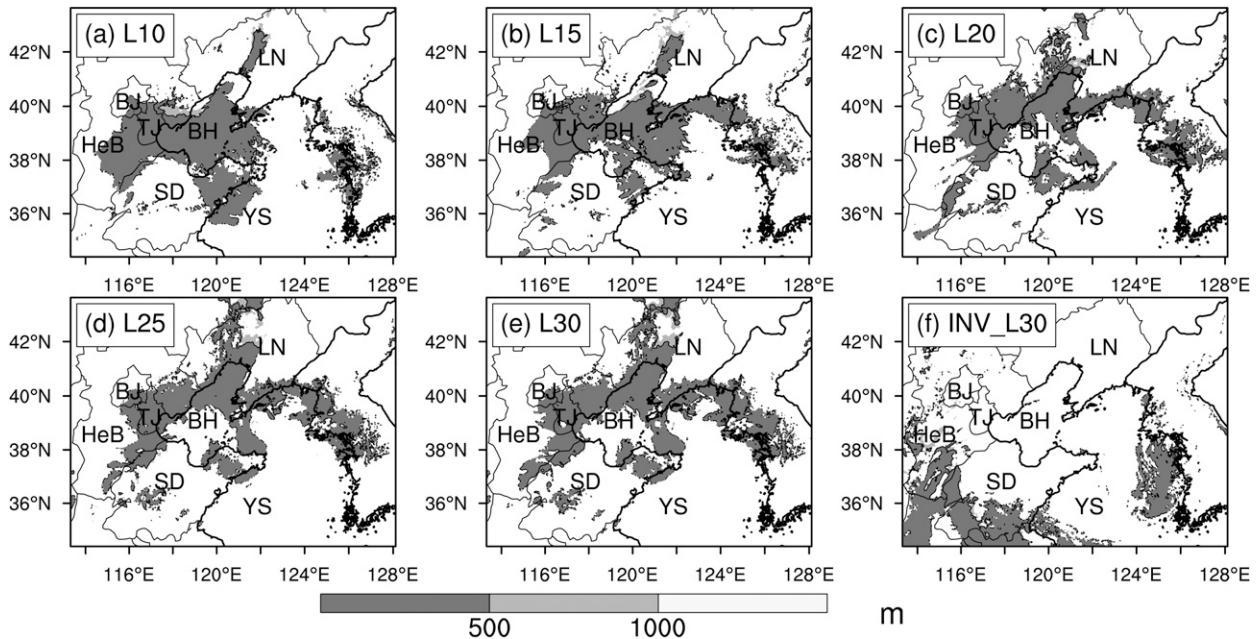
FIG. 8. As in Fig. 4, but for experiments L10, L15, L20, L25, L30, and INV_L30 in REPEXP.

All_1 to All_9 are plotted (Figs. 7a,b). With linearly increasing IC differences added to the IC of the WSEM, the sim-ETS (Fig. 7a) monotonically increases from −0.042 to 0.542, and the sim-bias (Fig. 7b) shows a general upward trend from 0.78 to 0.96 (from the WSEM to All_9). This implies that the improvement in the simulation due to the linear improvement of ICs is monotonic in this case. This monotonic behavior is significantly different from the nonlinearity of predictability documented by Melhauser and Zhang (2012) in their study of mesoscale convection.

2) REPLACEMENT EXPERIMENT (REPEXP)

As fog occurs in the atmospheric boundary layer (Cotton et al. 2010), it is hypothesized that IC differences at lower vertical model levels play a more important role in fog simulation. To test this hypothesis, the REPEXP documented in section 3 is performed.

Figure 8 shows the simulated fog coverage from five simulations (L10, L15, L20, L25, and L30) of REPEXP. The simulated fog coverage changed dramatically from the WSEM (Fig. 5) to L10 (Fig. 8a).The simulated fog coverage of experiments L10–L30 became closer to that of the BSTM (Fig. 5). The false fog coverage over the southern BH, YS, and the center of HB in L10 disappeared gradually by L30, and the small fog coverage over the center of LN (Fig. 8a) extended over a large area. Quantitatively, the sim-ETS and sim-bias results are calculated and plotted (Figs. 7c,d). The sim-ETS

increased rapidly from −0.042 to 0.249 from the WSEM to L10, and then continued to increase to 0.354, 0.509, and 0.791 for L15, L20, and L25, respectively, with a slow increase to 0.839 for L30. The sim-bias increased rapidly from 0.78 to 0.96 from the WSEM to L10, and then stayed stable at a value between 0.93 and 0.99 for L15, L20, L25, and L30. This implies that the IC differences at lower levels play a more important role in fog simulation in this case, which verified our hypothesis.

To verify the reliability of the REPEXP, an experiment is conducted by adding the IC differences at the top 11 levels of the model (i.e., levels 30–40) to the IC of the WSEM to obtain a simulation (INV_L30). The simulated fog coverage of INV_L30 (Fig. 8f) is very similar to that of WSEM (Fig. 5). The sim-ETS and sim-bias for INV_L30 are −0.043 and 0.76 (very close to those of the WSEM: −0.042 for SWSEM-ETS and 0.78 for SWSEM-bias). These results further confirmed the importance of the IC differences at lower vertical model levels in this case.

3) REMOVAL EXPERIMENT (RMVEXP)

This section includes two subsections. In section 5c(3)i, the relative importance of the IC differences among Q_v, θ, and (U, V) for fog simulation in this case is explored by RMVEXP. In section 5c(3)ii, for variables showing the most sensitivity in RMVEXP as discussed in section 5c(3)i, the sensitivity to linear changes of their IC differences
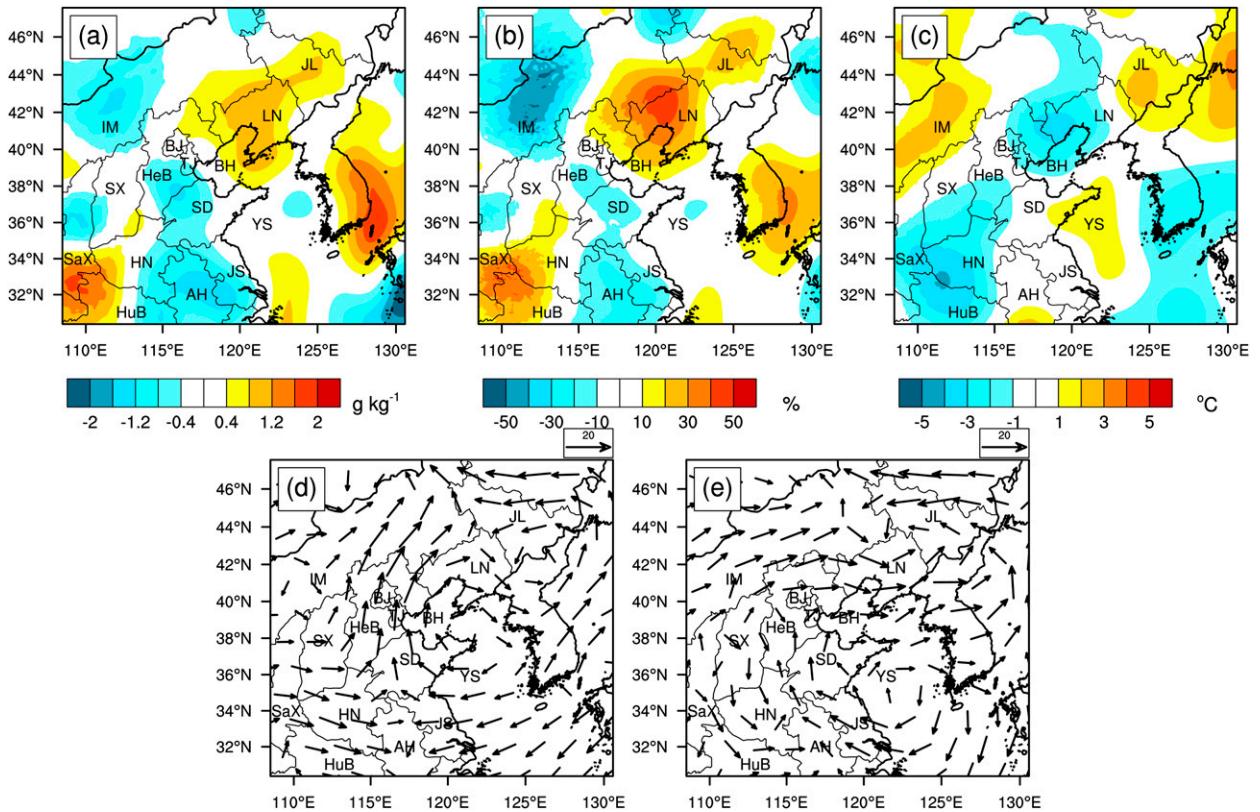
FIG. 9. The IC differences (BSTM − WSEM) of (a) water vapor mixing ratio (g kg^{-1}), (b) relative humidity (%), (c) temperature (°C), (d) horizontal wind (reference vector = 20 m s^{-1}), and (e) horizontal wind of the BSTM in D02 at lev3.

are further tested in detail by three additional groups of sensitivity experiments.

(i) Results of RMVEXP

As initial temperature, RH, winds, as well as advection, are all important factors in fog simulation and evolution (Zhou 2011; Zhou and Ferrier 2008), the RMVEXP (documented in section 3) is designed to examine the relative importance of the water vapor mixing ratio, potential temperature, and horizontal wind. In preparation for exploring the relative importance of IC differences for those three selected meteorological variables, in Fig. 9, we show the IC differences (BSTM − WSEM) of the water vapor mixing ratio, relative humidity, temperature, and horizontal wind at lev3 in D02. Comparing to the IC of the WSEM, the IC of the BSTM has a warm dry anomaly over Inner Mongolia (IM); cold moist anomalies over LN, BH, and Shaanxi Province (SaX); and a warm moist anomaly over YS (Figs. 9a–c). As for the horizontal wind, the BSTM captures the prevailing southerly wind over NC and the convergence zone to the south (Figs. 9d,e). This implies that, in this case, the warm moist air from the Yellow Sea is transported landward and contributes to the formation of the dense fog.

Figure 10 shows the simulated fog coverage of RMVEXP and the results are summarized in Table 1. The simulated fog coverage shows that removing the IC differences (the good information) from potential temperature (RMV_θ) and horizontal wind (RMV_UV) makes the most contribution to the failure of fog simulations in this case. Quantitatively, Figs. 7e,f show the sim-ETS and sim-bias calculated for these runs. According to Fig. 7, if the IC differences of potential temperature (RMV_θ) or horizontal wind (RMV_UV) were removed individually, the sim-ETS is clearly lower than that of the water vapor mixing ratio (RMV_Qv). If the IC differences of the potential temperature (RMV_θ, RMV_Qvθ, RMV_θ UV and RMV_Qvθ UV) were removed, the sim-bias is systematically lower than that of the other experiments in the RMVEXP. If the IC differences of potential temperature and horizontal wind combined were removed (RMV_θ UV and RMV_Qvθ UV), the sim-ETS values of RMV_θ UV and RMV_Qvθ UV were −0.036 and −0.040, respectively, which is very close to that of the WSEM (−0.042). This implies that the IC differences of potential temperature and horizontal wind played more significant roles than that of the water vapor mixing ratio in fog simulation in this case.
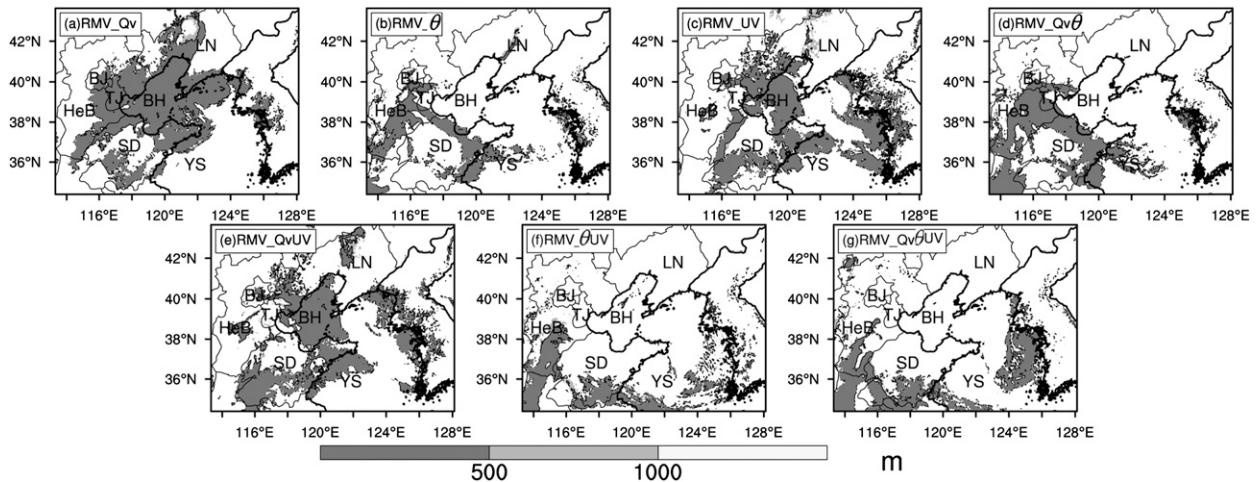
FIG. 10. As in Fig. 4, but for experiments (a) RMV_Qv, (b) RMV_θ, (c) RMV_UV, (d) RMV_Qvθ, (e) RMV_QvUV, (f) RMV_θ UV, and (g) RMV_Qvθ UV in RMVEXP.

(ii) Additional RMV sensitivity experiments

To further test the improvement due to individual changes of potential temperature and horizontal wind in the ICs, we use a similar approach as in experiments All_1 to All_9. We split the IC differences into five equal parts and create "intermediate" ICs with changes only in potential temperature and/or horizontal wind. Three groups of experiments are obtained and the naming of these experiments follows the previous convention: RMV_θ_n adds back $n/5$ of the potential temperature difference to RMV_θ. The simulated fog coverage in Fig. 11 shows that with linear improvement of potential temperature and/or horizontal wind in ICs, there is a monotonic improvement in the simulation (Figs. 11a–d, 11e–h, and 11i–l). Through comparing the simulated fog coverage among the three groups of experiments and that of the SPTEXP (corresponding to All_2, All_4, All_6, and All_8), it was found that the simulated fog coverage for RMV_θ UV_1 to RMV_θ UV_4 was much closer to that of the SPTEXP than these of RMV_θ_1 to RMV_θ_4 and RMV_UV_1 to RMV_UV_4. Quantitatively, the sim-ETS (sim-bias) results for these three groups of experiments were calculated and plotted (Fig. 12). With the linear improvement of ICs due to linearly improving the field of the potential temperature and/or the horizontal wind, the sim-ETS (Figs. 12a,c,e) increases monotonically, and the sim-bias (Figs. 12b,d,f) also trends toward unity with improved ICs, which is consistent with the results of the SPTEXP (corresponding to All_2, All_4, All_6, and All_8; Figs. 7a,b). In particular, the values of sim-ETS and sim-bias for RMV_θ UV_1 to RMV_θ UV_4 are very close to those of the SPTEXP. This suggests that there is monotonic improvement in the

simulation with improvement of each of the dependent variables separately. Moreover, the improvement in the simulation due to the linear improvement of the ICs for both potential temperature and horizontal wind is notable in this case.

6. Discussion

In this section, the physical interpretation is given for the results obtained in section 5b, namely 1) the improvement in the simulations due to the linear improvement of the ICs is monotonic in this case, 2) IC differences at lower levels are of more influence to the simulation than those of the upper vertical model levels in this case, and 3) improvements in potential temperature and horizontal wind are more important than those of the water vapor mixing ratio in this case.

The evolution of simulated fog coverage for BSTM and WSEM is displayed in Fig. 13. In BSTM, fog coverage first appeared at 1200 UTC 20 February 2007 over BH and extended to NC and northern BH at 0300 UTC

TABLE 1. Summary of the simulated fog coverage of RMVEXP (shown in Fig. 10).

RMVEXP	Fig. 10 panel	Fog coverage over NC	False fog coverage	Missed fog coverage
RMV_Qv	a	Yes	BH	—
RMV_θ	b	Yes	—	BH, NC
RMV_UV	c	Yes	BH, YS, SD	LN
RMV_Qvθ	d	Yes	SD, HN	BH, LN
RMV_QvUV	e	Yes	BH, YS, SD	LN
RMV_θ UV	f	No	BH, SD	NC, BH
RMV_Qvθ UV	g	No	YS, SD	NC, BH

FIG. 11. As in Fig. 4, but for experiments (a)–(d) RMV_θ_1 to RMV_θ_4, (e)–(h) RMV_UV_1 to RMV_UV_4, and (i)–(l) RMV_θUV_1 to RMV_θUV_4.

21 February 2007. Meanwhile, NC was dominated by southerly wind as fog started to form (Fig. 13a). By contrast, WSEM did not produce the same evolution as BSTM, and the same area is dominated by northerly wind instead (Fig. 13b). This change in wind direction in the worst member prevents the transport of moist air from ocean to land. So we fixed a box (indicated in Figs. 13a10 and 13b10) over this area, and the following analyses of evolution and budget are conducted over the area of this box.

Figure 14a shows the evolution of area-average meteorological variables (θ, Qv, and RH) for the BSTM and WSEM simulations from 0000 UTC 20 February (the initial time) to 0300 UTC 21 February 2007 (the mature stage of the fog event) every 12 min over the area of the box at lev3. Compared to the WSEM, the BSTM has a much warmer and moister air mass over NC during fog formation.

To further understand the underlying physics, we perform budget analyses of the area-average potential temperature and water vapor mixing ratio over the area of the box at lev3 (Golding 1993; Guedalia and Bergot 1994; Tardif 2007). In WRF, the prognostic equations of θ and Qv are as follow (http://www.atmos.washington.edu/~scavallo/wrf_thermo.pdf; Chen and Dudhia 2000; Skamarock et al. 2008):

$$\partial_t\theta = -m_x m_y[\partial_x(U\theta) + \partial_y(V\theta)] - m_y\partial_\eta(\Omega\theta) + F_\theta \quad (5)$$

and

$$\partial_t\mathrm{Qv} = -m_x m_y[\partial_x(U\mathrm{Qv}) + \partial_y(V\mathrm{Qv})] - m_y\partial_\eta(\Omega\mathrm{Qv}) + F_{\mathrm{Qv}}, \quad (6)$$

where $-m_x m_y[\partial_x(U\alpha) + \partial_y(V\alpha)]$, $-m_y\partial_\eta(\Omega\alpha)$, and F_α represent the horizontal advection term, the vertical transport term, and the forcing term from the parameterized physics of quantity α, respectively. According to the option of physical parameterization schemes in this study, the forcing term for θ includes a radiation term [R(Rat)], a turbulence term [R(tur)], and a condensation and evaporation term [R(LC)], while the forcing term for Qv includes a turbulence term [R(tur)] and a condensation and evaporation term [R(LC)]. If the two terms $-m_x m_y[\partial_x(U\alpha) + \partial_y(V\alpha)]$ and $-m_y\partial_\eta(\Omega\alpha)$ are regarded as the advection term [R(Adv)], the tendency equations of θ and Qv can be written as

$$\partial_t\theta = R(\mathrm{Rat}) + R(\mathrm{Tur}) + R(\mathrm{LC}) + R(\mathrm{Adv}) \quad (7)$$

and

$$\partial_t\mathrm{Qv} = R(\mathrm{Tur}) + R(\mathrm{LC}) + R(\mathrm{Adv}). \quad (8)$$

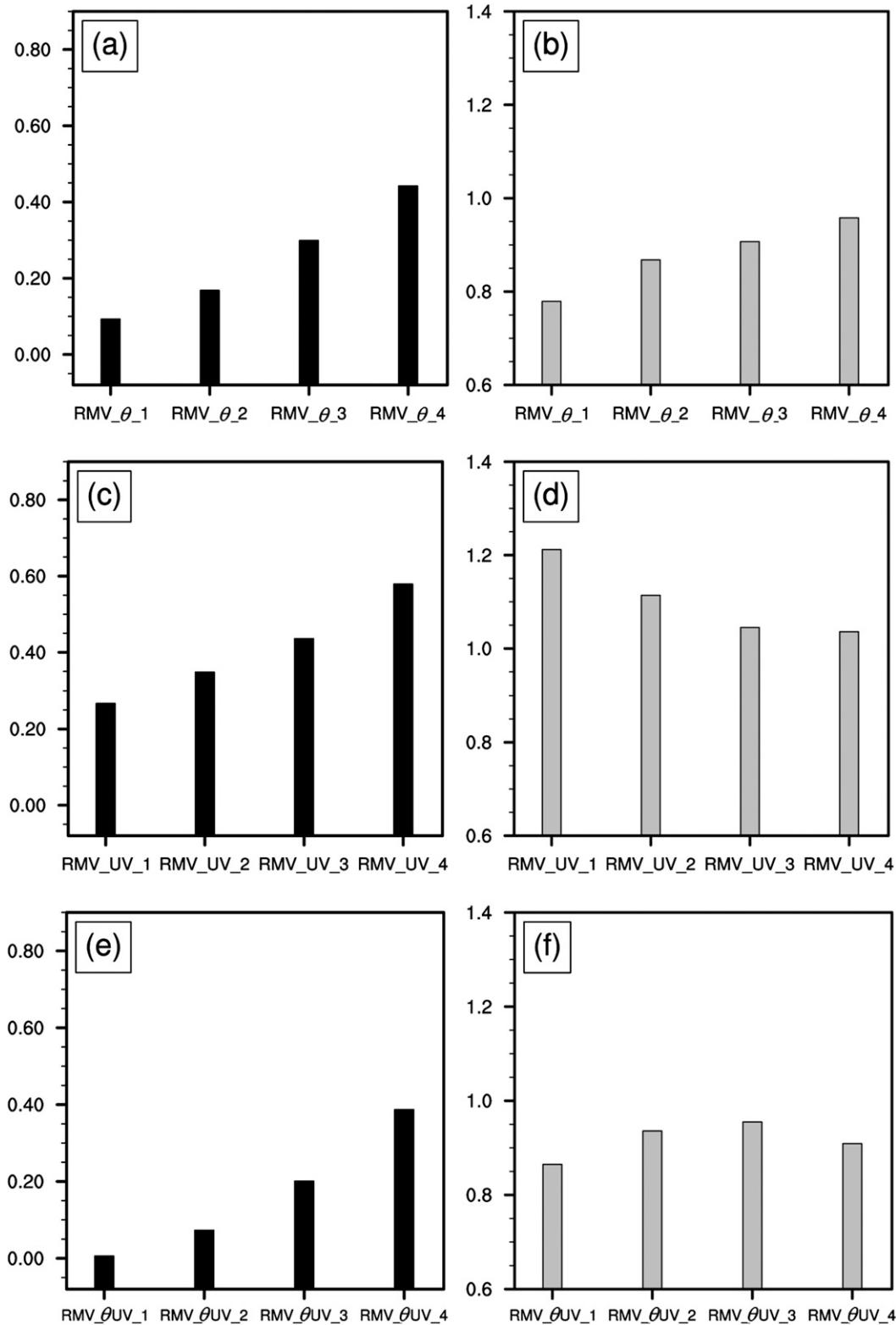All these terms are obtained directly from the WRF output after adding the output of the individual terms to

FIG. 12. As in Fig. 7, but for experiments (a),(b) RMV_θ_1 to RMV_θ_4; (c),(d) RMV_UV_1 to RMV_UV_4; and (e),(f) RMV_θ UV _1 to RMV_θ UV _4.
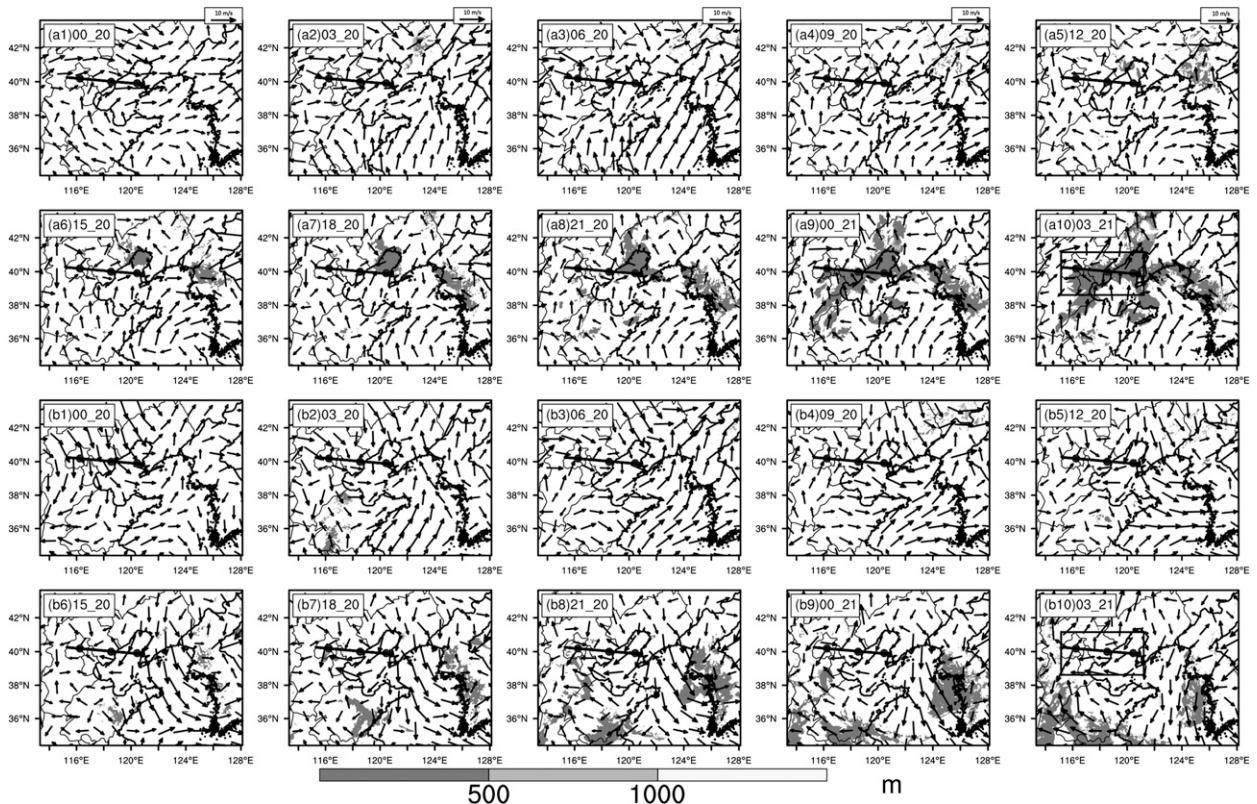
FIG. 13. The simulated fog coverage (shading) at lev3 and surface wind (vector, reference vector = $10\,\mathrm{m\,s^{-1}}$) evolution for the (a) BSTM and (b) WSEM in D03. The 3-hourly maps from 0000 UTC 20 Feb to 0300 UTC 21 Feb 2007 are shown.

the WRF codes and recompiling those codes. The units of $\partial_t\theta$ and $\partial_t Qv$ are kelvin per second and gram per kilogram per second, respectively. Figures 15a,b show the budgets of area-average θ (Fig. 15a) and Qv (Fig. 15b) for the BSTM (meshed) and the WSEM (solid) evaluated from WRF output at four typical times (the navy blue vertical straight dashed lines in Fig. 14), namely 0312 UTC 20 February (daytime), 1100 UTC 20 February (the period surrounding the maximum of area-average θ and Qv for both BSTM and WSEM), 1800 UTC 20 February (nighttime), and 0236 UTC 21 February 2007 (the period of the mature stage of fog in the BSTM), respectively. In Figs. 15a,b, note that both the total contribution for the BSTM (Totb, meshed black bar) and the WSEM (Totw, solid black bar) agreed well with the evolution of area-average θ and Qv (Fig. 14a), respectively. For area-average θ (Fig. 15a), the turbulence mixing and advection terms dominate the daytime and radiative cooling and advection terms dominate the nighttime. During the daytime just before fog formation, the BSTM has larger turbulence mixing and warmer advection than the WSEM. This is consistent with the higher increasing rate of area-average θ observed in Fig. 14a. What really discriminates the BSTM from the WSEM is the forcings during the

nighttime. For the BSTM, advection balances radiative cooling, so that the total forcing is close to zero (1100 UTC 20 February 2007 in Fig. 15a), while the WSEM has advection forcing in the opposite direction that causes the increase in the negative potential temperature tendency. This results in the faster potential temperature decrease for the WSEM than that of the BSTM (Fig. 14a). For area-average Qv (Fig. 15b), the contribution of condensation and evaporation (blue bar) is negligible, but large differences exist in the contributions of turbulence mixing and advection between the BSTM and the WSEM. Also, at 1100 UTC 20 February 2007, the dry advection in the WSEM made the major contribution to the total negative contribution to the water vapor mixing ratio in the WSEM. So a brief conclusion could be given that turbulence mixing and advection played the major role in fog simulation in this case. The dry cold advection was the major reason for the failure of the fog simulation of the WSEM in this case.

In Figs. 16a,b we see that larger inhomogeneities in temperature near the surface and lower wind speed at the initial time for the BSTM may be reasons for the enhancement in turbulence mixing for the BSTM at the initial time (observed in Fig. 15a). Furthermore, the
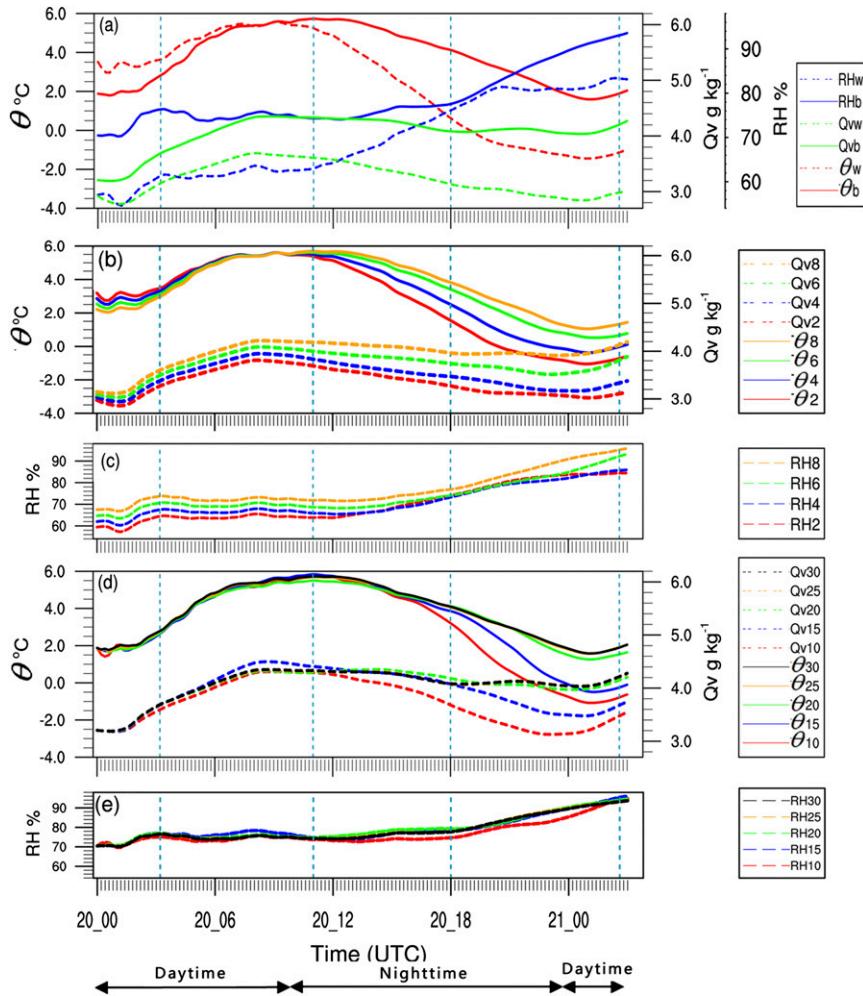
FIG. 14. (a) The time evolution of average θ (red, °C), Qv (green, g kg^{-1}), and RH (blue, %) for the BSTM (solid) and the WSEM (dashed). The time evolution of average θ (solid) and Qv (dashed) for (b) experiments All_2, All_4, All_6, and All_8 in SPTEXP and (d) experiments L10, L15, L20, L25, and L30 in REPEXP. The time evolution of average RH for (c) experiments All_2, All_4, All_6, and All_8 in SPTEXP and (e) experiments L10, L15, L20, L25, and L30 in REPEXP from 0000 UTC 20 Feb to 0300 UTC 21 Feb 2007 over the area shown as black rectangle in Fig. 13 at lev3.

correct turbulence mixing for the BSTM ensures the formation of an inversion for the BSTM (figures not shown). In Figs. 16c,d, we observe that NC was influenced mainly by a strong northwesterly cold current from Inner Mongolia for the WSEM (and this strong cold advection from the northern continued; figures not shown), while NC was influenced by both a cold current from the northwest and a southeasterly warm current from the Bohai Sea for the BSTM (and this situation continued; figures not shown), which agreed well with the higher area-average θ and lower area-average Qv for BSTM than that of the WSEM at the initial time (Fig. 14a). This implies that the initial fields of potential temperature and horizontal wind

play a more important role than water vapor mixing ratio in the fog simulation in this case (result 3 stated at the beginning of this section).

For the result of SPTEXP (result 1 stated at the beginning of this section), the evolution of area-average θ (Fig. 14b, solid line), Qv (Fig. 14b, dashed line), and RH (Fig. 14c) from All_2 to All_8 changed monotonically. One time (1800 UTC 20 February 2007) was shown here to represent the characteristics of the individual contributions to the area-average θ and Qv (Figs. 15c,d) for experiments from All_2 to All_8. It was clearly shown that the advection term played the major role in the total contributions to both the area-average θ and Qv. Meanwhile,
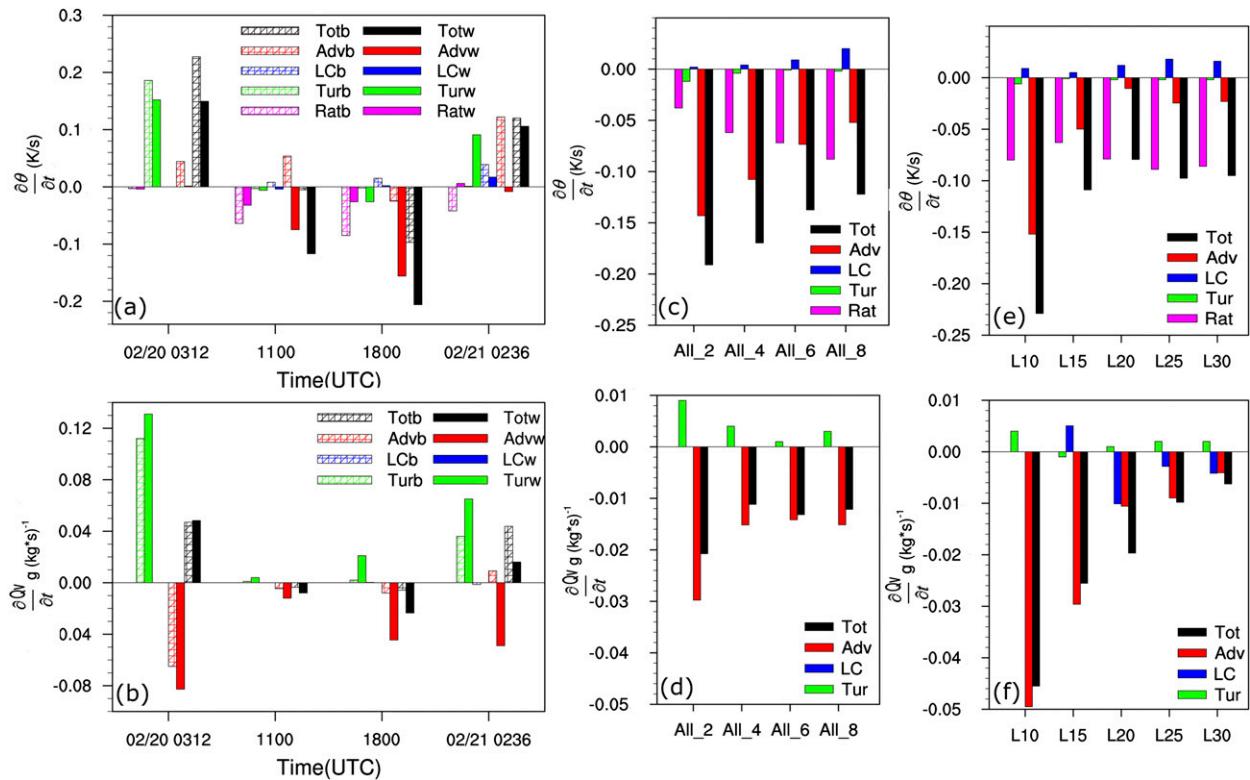
FIG. 15. The budgets of average (top) θ and (bottom) Qv over the area shown by the black rectangle in Fig. 13 at lev3: (a),(b) at 0312 UTC 20 Feb, 1100 UTC 20 Feb, 1800 UTC 20 Feb, and 0236 UTC 21 Feb 2007, with a solid (meshed) bar for the WSEM (BSTM). Budgets at 1800 UTC 20 Feb 2007 are shown for experiments (c),(d) All_2 to All_8 in SPTEXP and (e),(f) L10–L30 in REPEXP.

the individual contribution of advection to both the area-average θ and Qv changed monotonically from the value close to that of the WSEM (in All_2) to the value close to that of the BSTM (in All_8). That was why the improvement in simulations due to the linear improvement of the ICs is monotonic in this case.

In the REPEXP experiments, from the evolution of area-average θ, Qv, and RH, from L10 to L30 (Fig. 14d, solid line, dashed line, and Fig. 14e, respectively), it can be seen that the general character of the evolution is from a state close to that of WSEM (in L10) to one close to that of BSTM (in L30). From the budget analysis, it was clearly shown that the advection term played the major role in the total contribution to both area-average θ and Qv (Figs. 15e,f). Meanwhile, from L10 to L30, the change in the total contributions and the contribution from advection followed very well. Moreover, the largest change in advection existed from L10 to L15 for both area-average θ and Qv. That is why IC differences at lower levels are of more importance to the simulation than that at the upper vertical model levels (result 2 stated at the beginning of this section).

7. Summary

This paper studies the predictability of a dense fog event that occurred over NC and had a severe impact on local transportation but was forecast poorly. To evaluate the predictability, ensemble sensitivity analysis (Melhauser and Zhang 2012) is performed based on 40-member ensemble simulations utilizing the Weather Research and Forecasting Model (WRF). The differences in initial conditions (ICs) between the best and worst ensemble members selected from the ensemble simulations are taken and parts of them are added to the IC of the worst member to evaluate the resulting improvement. Also based on the IC differences, the ICs for only certain model levels or meteorological variables are changed to test the level and variable dependency. The results from the sensitivity experiments are concluded as follows.

1) The linear improvement in ICs yields monotonic improvements in the simulation result in this case. It is interesting that although fog simulations are highly sensitive to IC differences, the predictability of the fog, which is tied to having the correct turbulence mixing and advection of temperature and moisture at
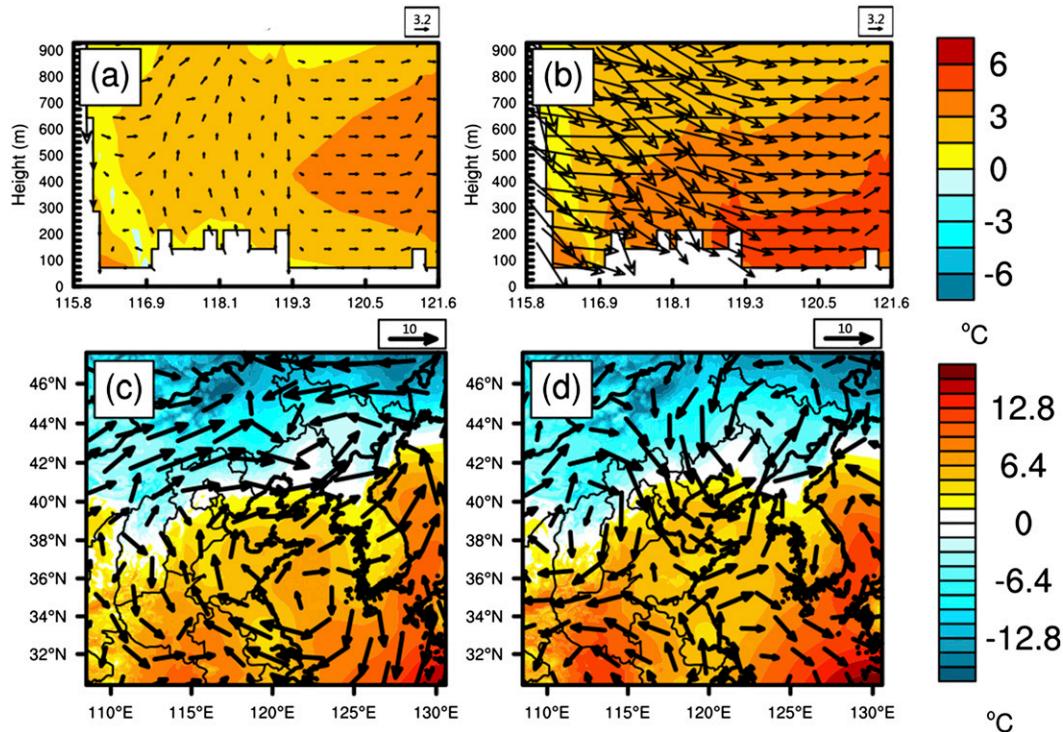
FIG. 16. The (a),(b) vertical cross sections and (c),(d) maps of wind and temperature for the (left) BSTM and (right) WSEM at lev3 in D02 at 0000 UTC 20 Feb 2007 (the initial time). The vertical cross section is along the line indicated in Fig. 13.

lower levels in this case, appears to be higher than for some other mesoscale phenomena, for example, mesoscale convection systems.

2) The lower levels have a greater impact on the fog simulation than the upper levels in this case.

3) The contributions from the potential temperature and horizontal wind are more important than that of the water vapor mixing ratio in this case. The improvement of the simulations due to the individual linear improvements in potential temperature and horizontal wind in the ICs is also monotonic in this case.

Using the budget analyses of potential temperature and water vapor mixing ratio, correct advection of temperature and moisture is found to be necessary for a correct simulation of the location of fog in this case. Furthermore, the monotonic improvement in the fog simulation results from the monotonic improvement of the advection term in the sensitivity experiments.

It is worth mentioning that the results of the sensitivity experiments shown in this paper do not change if we use the second-best (M30) and worst (M38) members from the ensemble (results not shown).

These results are primary and helpful for targeting observations in research to determine sensitive regions and to improve fog forecasting. However, this study is only an initial attempt to explore the sensitivity of fog simulations to IC differences using ensemble-based sensitivity tests, and the following two issues should be considered in future studies to obtain more persuasive conclusions. First, our studies were based on the assumption that the model is perfect. All of the sensitivity experiments in this paper were based on a single-model ensemble simulation, which cannot take the model uncertainty into consideration. Further studies utilizing multimodel ensemble simulations, which include model uncertainty (Zhou and Du 2010), should be performed. Second, more advection fog events over the NC region should be investigated before the conclusions can be confirmed. The conclusions from the sensitivity study in this paper should also be verified by the assimilation of real data. We intend to address all of the above issues in future work.

REFERENCES

Ancell, B., and G. J. Hakim, 2007: Comparing adjoint-and ensemble-sensitivity analysis with applications to observation targeting. *Mon. Wea. Rev.,* **135,** 4117–4134, doi:10.1175/2007MWR1904.1.

Ballard, S., B. Golding, and R. Smith, 1991: Mesoscale model experimental forecasts of the haar of northern Scotland. *Mon. Wea. Rev.,* **119,** 2107–2123, doi:10.1175/1520-0493(1991)119<2107:MMEFOT>2.0.CO;2.

Bergot, T., and D. Guedalia, 1994: Numerical forecasting of radiation fog. Part I: Numerical model and sensitivity tests. *Mon. Wea. Rev.,* **122,** 1218–1230, doi:10.1175/1520-0493(1994)122<1218:NFORFP>2.0.CO;2.

——, D. Carrer, J. Noilhan, and P. Bougeault, 2005: Improved site-specific numerical prediction of fog and low clouds: A feasibility study. *Wea. Forecasting,* **20,** 627–646, doi:10.1175/WAF873.1.

Chen, S., and J. Dudhia, 2000: Annual report: WRF physics. Air Force Weather Agency, 38 pp. [Available online at http://www.mmm.ucar.edu/wrf/users/docs/wrf-doc-physics.pdf.]

Chibe, R. J., and W. R. Cotton, 2003: The numerical simulation of fog with the RAMS@ CSU cloud-resolving mesoscale forecast model. Atmospheric Science Paper 741, Dept. of Atmospheric Science, Colorado State University, 109 pp.

Cotton, W. R., G. Bryan, and S. C. Van den Heever, 2010: *Storm and Cloud Dynamics*. 2nd ed. Academic Press, 820 pp.

Dudhia, J., 1989: Numerical study of convection observed during the Winter Monsoon Experiment using a mesoscale two-dimensional model. *J. Atmos. Sci.,* **46,** 3077–3107, doi:10.1175/1520-0469(1989)046<3077:NSOCOD>2.0.CO;2.

Duynkerke, P. G., 1991: Radiation fog: A comparison of model simulation with detailed observations. *Mon. Wea. Rev.,* **119,** 324–341, doi:10.1175/1520-0493(1991)119<0324:RFACOM>2.0.CO;2.

Errico, R., and T. Vukicevic, 1992: Sensitivity analysis using an adjoint of the PSU–NCAR mesoscale model. *Mon. Wea. Rev.,* **120,** 1644–1660, doi:10.1175/1520-0493(1992)120<1644:SAUAAO>2.0.CO;2.

Fitzjarrald, D. R., and G. G. Lala, 1989: Hudson Valley fog environments. *J. Appl. Meteor.,* **28,** 1303–1328, doi:10.1175/1520-0450(1989)028<1303:HVFE>2.0.CO;2.

Gao, S., Y. Qi, S. Zhang, and G. Fu, 2010: Initial conditions improvement of sea fog numerical modeling over the Yellow Sea by Using Cycling 3 DVAR Part I: WRF Numerical Experiments (in Chinese). *Periodical Ocean Univ. China,* **40** (10), 1–9.

Glickman, T., Ed., 2000: *Glossary of Meteorology*. 2nd ed. Amer. Meteor. Soc., 855 pp. [Available online at http://glossary.ametsoc.org/.]

Golding, B., 1993: A study of the influence of terrain on fog development. *Mon. Wea. Rev.,* **121,** 2529–2541, doi:10.1175/1520-0493(1993)121<2529:ASOTIO>2.0.CO;2.

Guedalia, D., and T. Bergot, 1994: Numerical forecasting of radiation fog. Part II: A comparison of model simulation with several observed fog events. *Mon. Wea. Rev.,* **122,** 1231–1246, doi:10.1175/1520-0493(1994)122<1231:NFORFP>2.0.CO;2.

Gultepe, I., and Coauthors, 2007: Fog research: A review of past achievements and future perspectives. *Pure Appl. Geophys.,* **164,** 1121–1159, doi:10.1007/s00024-007-0211-x.

Guo, L., and S. Zhang, 2007: Formative characteristics and its change of fog in central coastal plain of Hebei Province (in Chinese). *J. Nanjing Inst. Meteor.,* **30,** 359–364.

Hitt, K. J., 1994: Refining 1970's land-use data with 1990 population data to indicate new residential development. Water Resources Investigations Rep. 94-4250, U.S. Geological Survey, 15 pp.

Hong, S. Y., and J. O. J. Lim, 2006: The WRF single-moment 6-class microphysics scheme (WSM6). *J. Korean Meteor. Soc.,* **42,** 129–151.

Kain, J. S., 2004: The Kain–Fritsch convective parameterization: An update. *J. Appl. Meteor.,* **43,** 170–181, doi:10.1175/1520-0450(2004)043<0170:TKCPAU>2.0.CO;2.

Kunkel, B. A., 1984: Parameterization of droplet terminal velocity and extinction coefficient in fog models. *J. Climate Appl. Meteor.,* **23,** 34–41, doi:10.1175/1520-0450(1984)023<0034:PODTVA>2.0.CO;2.

Li, Y., A. Liang, Z. Zhang, Y. Luo, K. Liu, and J. Huang, 2007: Simulation and analysis of a winter advection fog in Beijing area (in Chinese). *J. Yunnan Univ. (Natural Sci. Edition),* **29,** 167–172.

Liang, A., Q. Zhang, H. Shen, K. Liu, X. Li, and J. Feng, 2009: The analysis and simulation of an advection fog event in Beijing (in Chinese). *J. Appl. Meteor. Sci.,* **20,** 612–621.

Melhauser, C., and F. Zhang, 2012: Practical and intrinsic predictability of severe and convective weather at the mesoscales. *J. Atmos. Sci.,* **69,** 3350–3371, doi:10.1175/JAS-D-11-0315.1.

Mlawer, E. J., S. J. Taubman, P. D. Brown, M. J. Iacono, and S. A. Clough, 1997: Radiative transfer for inhomogeneous atmospheres: RRTM, a validated correlated-k model for the longwave. *J. Geophys. Res.,* **102,** 16 663–16 682, doi:10.1029/97JD00237.

Muller, M., 2006: Numerical simulation of fog and radiation in complex terrain. Ph.D. thesis, University of Basel, Stratus 12, 90 pp.

——, C. Schmutz, and E. Parlow, 2007: A one-dimensional ensemble forecast and assimilation system for fog prediction. *Pure Appl. Geophys.,* **164,** 1241–1264, doi:10.1007/s00024-007-0217-4.

Musson-Genon, L., 1987: Numerical simulation of a fog event with a one-dimensional boundary layer model. *Mon. Wea. Rev.,* **115,** 592–607, doi:10.1175/1520-0493(1987)115<0592:NSOAFE>2.0.CO;2.

Nakanishi, M., 2000: Large-eddy simulation of radiation fog. *Bound.-Layer Meteor.,* **94,** 461–493, doi:10.1023/A:1002490423389.

Niu, S., C. Lu, H. Yu, L. Zhao, and J. Lu, 2010: Fog research in China: An overview. *Adv. Atmos. Sci.,* **27,** 639–662, doi:10.1007/s00376-009-8174-8.

Pagowski, M., I. Gultepe, and P. King, 2004: Analysis and modeling of an extremely dense fog event in southern Ontario. *J. Appl. Meteor.,* **43,** 3–16, doi:10.1175/1520-0450(2004)043<0003:AAMOAE>2.0.CO;2.

Roman-Cascon, C., C. Yague, M. Sastre, G. Maqueda, F. Salamanca, and S. Viana, 2012: Observations and WRF simulations of fog events at the Spanish Northern Plateau. *Adv. Sci. Res.,* **8,** 11–18, doi:10.5194/asr-8-11-2012.

Roquelaure, S., and T. Bergot, 2008: A local ensemble prediction system for fog and low clouds: Construction, Bayesian model averaging calibration, and validation. *J. Appl. Meteor. Climatol.,* **47,** 3072–3088, doi:10.1175/2008JAMC1783.1.

Ryerson, W. R., 2012: Toward improving short-range fog prediction in data-denied areas using the Air Force Weather

Agency mesoscale ensemble. Ph.D. thesis, Naval Post-graduate School, 225 pp. [Available online at http://www.dtic.mil/cgi-bin/GetTRDoc?AD=ADA567345.]

Skamarock, W. C., and Coauthors, 2008: A description of the Advanced Research WRF version 3. NCAR Tech. Note NCAR/TN–475+STR, 113 pp.

Sukoriansky, S., B. Galperin, and V. Perov, 2005: Application of a new spectral theory of stably stratified turbulence to the atmospheric boundary layer over sea ice. *Bound.-Layer Meteor.,* **117,** 231–257, doi:10.1007/s10546-004-6848-4.

Tardif, R., 2007: The impact of vertical resolution in the explicit numerical forecasting of radiation fog: A case study. *Pure Appl. Geophys.,* **164,** 1221–1240, doi:10.1007/s00024-007-0216-5.

Torn, R. D., and G. J. Hakim, 2008: Ensemble-based sensitivity analysis. *Mon. Wea. Rev.,* **136,** 663–677, doi:10.1175/2007MWR2132.1.

——, and ——, 2009: Initial condition sensitivity of western Pacific extratropical transitions determined using ensemble-based sensitivity analysis. *Mon. Wea. Rev.,* **137,** 3388–3406, doi:10.1175/2009MWR2879.1.

Van der Velde, I., G. Steeneveld, B. Wichers Schreur, and A. Holtslag, 2010: Modeling and forecasting the onset and duration of severe radiation fog under frost conditions. *Mon. Wea. Rev.,* **138,** 4237–4253, doi:10.1175/2010MWR3427.1.

Van Sang, N., R. K. Smith, and M. T. Montgomery, 2008: Tropical-cyclone intensification and predictability in three dimensions. *Quart. J. Roy. Meteor. Soc.,* **134,** 563–582, doi:10.1002/qj.235.

von Glasow, R., and A. Bott, 1999: Interaction of radiation fog with tall vegetation. *Atmos. Environ.,* **33,** 1333–1346, doi:10.1016/S1352-2310(98)00372-0.

Walser, A., D. Luthi, and C. Schar, 2004: Predictability of precipitation in a cloud-resolving model. *Mon. Wea.*

Rev., **132,** 560–577, doi:10.1175/1520-0493(2004)132<0560:POPIAC>2.0.CO;2.

Welch, R., M. Ravichandran, and S. Cox, 1986: Prediction of quasi-periodic oscillations in radiation fogs. I: Comparison of simple similarity approaches. *J. Atmos. Sci.,* **43,** 633–651, doi:10.1175/1520-0469(1986)043<0633:POQPOI>2.0.CO;2.

Wu, D., Z. Meng, and D. Yan, 2013: The predictability of a squall line in South China on 23 April 2007. *Adv. Atmos. Sci.,* **30,** 485–502, doi:10.1007/s00376-012-2076-x.

Zhang, C. L., S. G. Miao, Q. C. Li, and F. Chen, 2007: Impacts of fine-resolution land use information of Beijing on a summer severe rainfall simulation (in Chinese). *Chin. J. Geophys.,* **50,** 1372–1382.

Zhang, F., C. Snyder, and R. Rotunno, 2003: Effects of moist convection on mesoscale predictability. *J. Atmos. Sci.,* **60,** 1173–1185, doi:10.1175/1520-0469(2003)060<1173:EOMCOM>2.0.CO;2.

——, A. M. Odins, and J. W. Nielsen-Gammon, 2006: Mesoscale predictability of an extreme warm-season precipitation event. *Wea. Forecasting,* **21,** 149–166, doi:10.1175/WAF909.1.

Zhou, B., 2011: Introduction to a new fog diagnostic scheme. NCEP Office Note 466, 43 pp. [Available online at www.emc.ncep.noaa.gov/officenotes/newernotes/on466.pdf.]

——, and B. S. Ferrier, 2008: Asymptotic analysis of equilibrium in radiation fog. *J. Appl. Meteor. Climatol.,* **47,** 1704–1722, doi:10.1175/2007JAMC1685.1.

——, and J. Du, 2010: Fog prediction from a multimodel mesoscale ensemble prediction system. *Wea. Forecasting,* **25,** 303–322, doi:10.1175/2009WAF2222289.1.

——, ——, I. Gultepe, and G. Dimego, 2012: Forecast of low visibility and fog from NCEP: Current status and efforts. *Pure Appl. Geophys.,* **169,** 895–909, doi:10.1007/s00024-011-0327-x.